Pergamon

Int. Comm. Heat Mass Transfer, Vol. 30, No. 3, pp. 369-378, 2003

0735–1933/03/$–see front matter

Available online at www.sciencedirect.com

SCIENCE DIRECT®

PII: S0735-1933(03)00055-1

A BLOCK-IMPLICIT METHOD FOR NUMERICAL SIMULATION OF SWIRLING FLOWS IN A MODEL COMBUSTOR

Marcelo J.S. de Lemos
Departamento de Energia - IEME
Instituto Tecnológico de Aeronáutica - ITA
12228-900 - São José dos Campos - SP - Brazil
E-mail: delemos@mec.ita.br

(Communicated by J.P. Hartnett and W.J. Minkowycz)

ABSTRACT

Numerical results for swirling flows obtained by a point-wise locally-implicit scheme are here reported. Computations are presented for incompressible laminar flow inside a model combustor. Governing equations are written in terms of the so-called primitive variables and are recast into a general form. Finite-differencing is obtained by means of the widely-used control-volume approach. Discretized cross-flow equations are applied to each cell face and then, together with the mass-continuity and the tangential momentum equations, are simultaneously solved by means of a direct method in each computational node. Residue histories for governing equations are presented. Advantages in using a coupled procedure when compared with standard segregated schemes are discussed.

Introduction

The use of numerical tools for solving real-world engineering problems has been a common-place strategy in the past decade, mainly due to the accelerated advances in microprocessor technologies and substantial improvements in software development. For the particular case of modern swirl-induced gas turbine combustors, these two factors have led to the reduction of required time for design and analysis of such devices. Ultimately, many different configurations are able to be analyzed in a short period of time, reducing them early uncertainties in prototype conception and evaluation.

In spite of the ever greater use of Computational Fluid Dynamics & Heat Transfer, the numerical solution of swirling flows is still a challenging task due to the intricate coupling between tangential- and radial-momentum equations. Accordingly, the rate of convergence of any algorithm is essentially dictated by the degree in which physical coupling is mimicked by the method in question. In the end, this is an

indication that numerical solutions of swirling flows, in most cases, suffer from the disadvantage of longer computing times when compared to their non-swirling counterpart. There seems to be then much need for development of coupled algorithms for such problems.

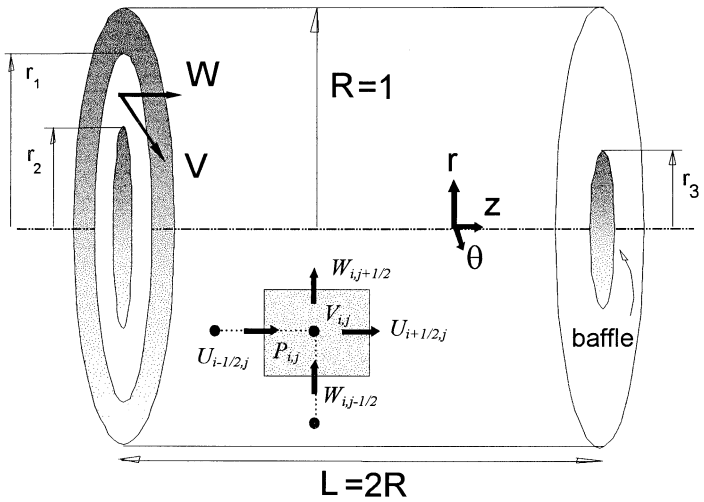

FIG. 1
Model combustor geometry and control-volume notation.

Most solutions found in the literature for swirling flows solve each variable independently, in a segregated fashion, until final convergence is obtained [1-3]. Usually, velocity components and pressure field are decoupled from each other with the employment of repetitive solution of a pressure or pressure-correction equation. A subsequent update for the velocity field completes one cycle in this iterative process. This strategy forms the basis of the SIMPLE family of algorithms [4,5,6].

In references [7,8], a predictive technique based on the work of Vanka [9,10] for coupled solution of the momentum and continuity equations has been applied to several flow configurations. There the method solves, for each computational cell, all momentum and continuity equations in an implicit manner. An essential characteristic of Vanka's work, the multigrid artifice, has not been used in [7,8] due to the relatively modest grids there analyzed. Multigrid techniques are known to perform well with mid-size to large grids, but are rather ineffective when applied to small size problems [11]. For this reason, no multigrid or any other large grid accelerating scheme was in [7,8] implemented.

The implicit handling of the pressure-velocity interaction, first proposed in [9,10], brings information from neighboring cells to the finite-volume immediately, increasing then overall convergence rates. Recently [12], the coulped method has been extended to buoyancy-driven cavity flows showing improvements in computer time requirements when an implicit scheme is also applied for handling the

temperature-velocity coupling. In the present context, a fully-implicit treatment is associated with the idea of simultaneously updating flow and scalar fields at each step within the error smoothing operator. To the best of the author's knowledge, in all published work, no tangential velocity field, seen here as *scalar*, is numerically treated in a fully implicit manner in the same way as considered below.

Based on the foregoing, the objective of the present contribution is to further develop the early work on coupled schemes, extending it now to a fully implicit algorithm for solving the axi-symmetric three-dimensional flow field occurring in model combustors. The tangential velocity V is no longer decoupled from the cross-flow (components U and W), so that the strong coupling due to the centripetal acceleration is directly accounted for in the method. In addition, the point-wise aspect of the error smoothing operator here proposed makes it attractive for use in more advanced computer architectures such as vector and parallel computers.

Geometry And Flow Equations

The geometry here considered, for the solution of the internal flow field, is schematically shown in FIG. 1. The combustor geometry is approximated by a circular duct of constant radius R. At inlet, the air-fuel mixture enters through a circular slot with clearance r_1-r_2. At one diameter downstream the entrance, a circular baffle of radius r_3 is located. Swirling flow, impaired by vanes located at the chamber inlet, is simulated by assuming a constant tangential velocity V_{in} at z=0. Also at inlet, a constant axial velocity W_{in} is considered.

The conservation equations for mass and momentum can then be written in a compact form if the existing analogies among the processes of accumulation, transport, convection and generation/destruction for the transported quantities are observed. This general equation can be written in its conservative two-dimensional laminar form as:

$$\frac{\partial}{\partial z}\left[\rho W\phi-\Gamma^{\phi}\frac{\partial\phi}{\partial z}\right]+\frac{1}{r}\frac{\partial}{\partial r}\left[r\left(\rho U\phi-\Gamma^{\phi}\frac{\partial\phi}{\partial r}\right)\right]=S^{\phi} \tag{1}$$

In Eq. (1) ϕ can represent any quantity of vectorial or scalar nature, ρ is the fluid density, U and W are the velocity components in the r- and z-directions, respectively, Γ_{ϕ} is the transport coefficient for diffusion and S_{ϕ} is the source term. TABLE 1 identifies correspondent terms for the different equations represented by Eq. (1). In both TABLE 1 and equation (1), axi-symmetry is considered.

TABLE 1
Terms in the general transport equation.

	ϕ	Γ^{ϕ}	S^{ϕ}
Continuity	1	0	0
Axial Momentum	W	μ	$-\frac{\partial P}{\partial z}$
Radial Momentum	U	μ	$-\left(\frac{\partial P}{\partial r}+\frac{\mu U}{r^2}-\frac{\rho V^2}{r}\right)$
Tangential Momentum	V	μ	$-\left(\frac{\mu V}{r^2}+\frac{\rho UV}{r}\right)$

Discretized Equations and Numerical Method

In this work, the set of equations for mass and momentum above is differentiated by means of the widely-used control-volume approach of Patankar [4]. In that method, the computational domain is divided into finite non-overlapping regions containing each region a computational node. A staggered grid arrangement is used in the present work due to its well-established advantages in calculating fluid flow problems [5]. FIG. 1 also illustrates the control-volume used along with relevant notation.

The differential equations are then integrated over each volume yielding a set of algebraic equations for each dependable variable. The tangential velocity V and pressure P are centered around the computational node (i,j). Cross-flow velocities U and W are assumed to prevail at cells faces as usually done in a staggered-grid arrangement. Internodal variation for the dependent variables can be of different kind corresponding to different Finite-Difference Formulation. In the present work, for simplicity, the Upwind Differencing Scheme is used to model convective fluxes across volume faces. However, the formulation below is presented in such way that no difficulties arise if another differencing scheme is employed.

The block-implicit arrangement below for the flow and continuity equations, as mentioned, was first presented in [9,10]. For the sake of completeness when extending it to swirling flows, the cross flow equations for U and W are here also included. Integrating then the continuity equation around point (i,j) of FIG. 1, following standard practices in numerical differentiation, one has [4],

$$F_{i+\frac{1}{2}}U_{i+\frac{1}{2},j} - F_{i-\frac{1}{2}}U_{i-\frac{1}{2},j} + F_{j+\frac{1}{2}}W_{i,j+\frac{1}{2}} - F_{j-\frac{1}{2}}W_{i,j-\frac{1}{2}} = 0 \tag{2}$$

where the geometric coefficients Fs can be interpreted as (area of flow)/(volume of computational node).

For the radial momentum equation, the final form for the $U_{i-\frac{1}{2},j}$ component contains coefficients representing influences by convection and diffusion mechanisms in addition to all sources and pressure gradient terms. The discretized equation reads,

$$a^u_{1-\frac{1}{2}}U_{i-\frac{1}{2},j} = \sum_{nb=1}^{4} a^u_{nb}U_{nb} + \frac{A_{i-\frac{1}{2}}}{\rho}\left[P_{i-1,j} - P_{i,j}\right] + S^U_C \tag{3}$$

where

$$a^u_{1-\frac{1}{2}} = \sum_{nb=1}^{4} a^u_{nb} - S^U_P\,; \quad S^U_P = -\left(\frac{\mu}{\rho}\right)\frac{1}{r_{i-\frac{1}{2}}}\,; \quad S^U_C = \frac{(V_{i-1,j}+V_{i,j})^2}{4r_{i-\frac{1}{2}}} \tag{4}$$

The source term in TABLE 1 was given the usual linearized form $S^U = S^U_C + S^U_P U_{i-\frac{1}{2}}$. Also, the coefficients a^u_{nb} appearing in Eq. (3) refers to neighbor nodal points and account for the contributions, at each face, of the mechanisms of convection and diffusion. For a variable ϕ and for the purely upwind formulation here considered its general form reads,

$$a_{nb}^{\phi} = \frac{\Gamma^{\phi}}{\rho}\frac{A_{nb}}{\delta r_{nb}} + \left\| A_{nb}U_{nb}, 0 \right\| \tag{5}$$

where and the operator $\|A,B\|$ means the greater between A and B, A_{nb} is the area of transport, U_{nb} the velocity prevailing over the control-volume face area A_{nb} and δr_{nb} the distance between adjacent control-volume centers.

The last term on Eq. (3) represents the discrete form of the *centripetal* acceleration shown in TABLE 1. For application in the numerical algorithm below, this source term, S_C^U, is split as,

$$S_C^U = \frac{(V_{i-1,j}+V_{i,j})^2}{4r_{i-\frac{1}{2}}} = \frac{(V_{i-1,j}^2 - V_{i,j}^2)}{4r_{i-\frac{1}{2}}} + \frac{(V_{i-1,j}+V_{i,j})}{2r_{i-\frac{1}{2}}}V_{i,j} \tag{6}$$

so that Eq. (3) can be further manipulated to give,

$$U_{i-\frac{1}{2},j} = \hat{U}_{i-\frac{1}{2},j} + \hat{d}_{i-\frac{1}{2}}\left[P_{i-1,j} - P_{i,j}\right] + \hat{e}_{i-\frac{1}{2}} + \hat{f}_{i-\frac{1}{2}}V_{i,j} \tag{7}$$

where

$$\hat{U}_{i-\frac{1}{2},j} = \frac{\sum_{nb=1}^{4} a_{nb}^{u}U_{nb}}{a_{i-\frac{1}{2}}^{u}}; \quad \hat{d}_{i-\frac{1}{2}} = \frac{A_{i-\frac{1}{2}}}{\rho a_{i-\frac{1}{2}}^{u}}; \quad \hat{e}_{i-\frac{1}{2}} = \frac{(V_{i-1,j}^2 - V_{i,j}^2)}{4a_{i-\frac{1}{2}}^{u}r_{i-\frac{1}{2}}}; \quad \hat{f}_{i-\frac{1}{2}} = \frac{(V_{i,j}+V_{i-1,j})}{2a_{i-\frac{1}{2}}^{u}r_{i-\frac{1}{2}}} \tag{8}$$

For the coupled treatment here presented, the explicit contribution of V in the source term of U is necessary, as will be seen below.

A similar equation for the axial velocity component $W_{i,j-\frac{1}{2}}$ is given by,

$$W_{i,j-\frac{1}{2}} = \hat{W}_{i,j-\frac{1}{2}} + \hat{d}_{j-\frac{1}{2}}\left[P_{i,j-1} - P_{i,j}\right] \tag{9}$$

where,

$$\hat{W}_{j-\frac{1}{2}} = \frac{\sum_{nb=1}^{4} a_{nb}^{w}W_{nb}}{a_{j-\frac{1}{2}}^{w}}, \quad \hat{d}_{j-\frac{1}{2}} = \frac{A_{j-\frac{1}{2}}}{\rho a_{j-\frac{1}{2}}^{w}} \tag{10}$$

Following a similar procedure for the V velocity component, a final finite-difference equation can be assembled in the following form,

$$a_{ij}^{V}V_{i,j} = \sum_{nb=1}^{4} a_{nb}^{V}V_{nb} + S_C^V \tag{11}$$

where

$$a_{ij}^{V} = \sum_{nb=1}^{4} a_{nb}^{V} - S_P^V; \quad S_P^V = -\left\{\frac{\mu}{\rho}\frac{1}{r_i^2} + \left\| \frac{(U_{i-\frac{1}{2}}+U_{i+\frac{1}{2}})}{2r_i}, 0 \right\|\right\}; \quad S_C^U = \left\| -\frac{(U_{i-\frac{1}{2}}+U_{i+\frac{1}{2}})}{2r_i}, 0 \right\| V_{i,j} \tag{12}$$

Here also the source term was given the linearized form $S^V = S_C^V + S_P^V V_{ij}$, accounting further for the fact that the value of the *Corriollis* acceleration might be positive or negative. For positive U values, this

acceleration is considered in the S_P^V coefficient whereas for negative radial velocity components an explicit treatment for the product -*UV* is adopted. For simplicity, equations (11) can be rearranged such that,

$$V_{i,j} = \hat{V}_{i,j} \tag{13}$$

$$\text{where } \hat{V}_{ij} = \frac{\sum_{nb=1}^{4} a_{nb}^V V_{nb} + S_C^V}{a_{ij}^V} \tag{14}$$

In Eq. (14) all right-hand-side terms of Eq. (13) are assembled for convenient use in the coupled scheme.

The Coupled Numerical Strategy

In order to set up a scheme to annihilate the residues for the flow equations, *corrections* are then defined as differences between *exact* and *approximate* variables and can be written as:

$$\begin{aligned}
U'_{i-\frac{1}{2},j} &= U_{i-\frac{1}{2},j} - U^*_{i-\frac{1}{2},j},\\
U'_{i+\frac{1}{2},j} &= U_{i+\frac{1}{2},j} - U^*_{i+\frac{1}{2},j},\\
W'_{i,j-\frac{1}{2}} &= W_{i,j-\frac{1}{2}} - W^*_{i,j-\frac{1}{2}},\\
W'_{i,j+\frac{1}{2}} &= W_{i,j+\frac{1}{2}} - W^*_{i,j+\frac{1}{2}},\\
P'_{i,j} &= P_{i,j} - P^*_{i,j},\\
V'_{i,j} &= V_{i,j} - V^*_{i,j}
\end{aligned} \tag{15}$$

where the subscripts, as in FIG. 1, identifies locations in the grid, the superscript " ′ " distinguishes corrections and the symbol "*" corresponds to previous iteration.

Residuals for all four cross-flow momentum, tangential velocity and continuity of mass equations are readily obtained by plugging the *approximate* values, given by Eq. (15), into Eqs. (7)-(9)-(13). Then, defining residuals as the difference between the right- and left-hand side of Eqs. (7)-(9)-(13), one has,

$$\begin{aligned}
R_{i-\frac{1}{2},j} &= \hat{U}_{i-\frac{1}{2},j} + \hat{d}_{i-\frac{1}{2}}\left[P_{i-1,j} - P^*_{i,j}\right] + \hat{e}_{i-\frac{1}{2}} + \hat{f}_{i-\frac{1}{2}} V^*_{i,j} - U^*_{i-\frac{1}{2},j}\\
R_{i+\frac{1}{2},j} &= \hat{U}_{i+\frac{1}{2},j} + \hat{d}_{i+\frac{1}{2}}\left[P^*_{i,j} - P_{i+1,j}\right] + \hat{e}_{i+\frac{1}{2}} + \hat{f}_{i+\frac{1}{2}} V^*_{i,j} - U^*_{i+\frac{1}{2},j}\\
R_{i,j-\frac{1}{2}} &= \hat{W}_{i,j-\frac{1}{2}} + \hat{d}_{j-\frac{1}{2}}\left[P_{i,j-1} - P^*_{i,j}\right] - W^*_{i,j-\frac{1}{2}}\\
R_{i,j+\frac{1}{2}} &= \hat{W}_{i,j+\frac{1}{2}} + \hat{d}_{j+\frac{1}{2}}\left[P^*_{i,j} - P_{i,j+1}\right] - W^*_{i,j+\frac{1}{2}}\\
R_{i,j} &= -F_{i+\frac{1}{2}} U_{i+\frac{1}{2},j} + F_{i-\frac{1}{2}} U_{i-\frac{1}{2},j} - F_{j+\frac{1}{2}} W_{i,j+\frac{1}{2}} + F_{j-\frac{1}{2}} W_{i,j-\frac{1}{2}}\\
R^V_{i,j} &= -V^*_{i,j} + \hat{V}_{i,j}
\end{aligned} \tag{16}$$

Note that in Eqn. (16) velocities and pressure outside the (*i,j*) volume are assumed as exact, since the decomposition (15) is not applied to them. Further, Eq. (15) is not applied to the $\hat{e}$ and $\hat{f}$ terms of Eq. (8).

To make this idea clear, on takes the west face of the control volume show in FIG. 1 as an example (see equation (7)). For that particular face, one has,

$$(U^* + U')_{i-\frac{1}{2},j} = \hat{U}_{i-\frac{1}{2},j} + \hat{d}_{i-\frac{1}{2}}\left[P_{i-1,j} - (P^* + P')_{i,j}\right] + \hat{e}_{i-\frac{1}{2}} + \hat{f}_{i-\frac{1}{2}}(V^* + V')_{i,j} \tag{17}$$

As mentioned, note that the decomposition detailed in Eq. (15) was not applied to the "pseudo-velocity" $\hat{U}_{i-\frac{1}{2},j}$ nor to the coefficients $\hat{e}$ - $\hat{f}$ or to the pressure located outside the control volume (*i,j*). This is an essential feature of the method as will be seen below. For a given set of guessed or "starred" variables, Eq. (7) yields a residue, $R_{i-\frac{1}{2},j}$, related to the incorrect velocity such that,

$$U^*_{i-\frac{1}{2},j} = \hat{U}_{i-\frac{1}{2},j} + \hat{d}_{i-\frac{1}{2}}\left[P_{i-1,j} - P^*_{i,j}\right] + \hat{e}_{i-\frac{1}{2}} + \hat{f}_{i-\frac{1}{2}}V^*_{i,j} - R_{i-\frac{1}{2},j} \tag{18}$$

Subtracting now Eq. (18) from Eq. (17), an equation for the correction U' is obtained in the form,

$$U'_{i-\frac{1}{2},j} + \hat{d}_{i-\frac{1}{2}}P'_{i,j} - \hat{f}_{i-\frac{1}{2}}V'_{i,j} = R_{i-\frac{1}{2},j} \tag{19}$$

An equivalent path to reach the same result is to start out with Eq. (3) and first expand the source term with a decompostion for $V_{i,j}$ into the form,

$$S^U_C = \frac{(V_{i-1,j} + V_{i,j})^2}{4r_{i-\frac{1}{2}}} \approx \frac{(V_{i-1,j} + V^*_{i,j})^2 + 2(V_{i-1,j} + V^*_{i,j})V'_{i,j} + \overbrace{(V'_{i,j})^2}^{\approx 0}}{4r_{i-\frac{1}{2}}} = \frac{(V_{i-1,j} + V^*_{i,j})^2}{4r_{i-\frac{1}{2}}} + \frac{(V_{i-1,j} + V^*_{i,j})}{2r_{i-\frac{1}{2}}}V'_{i,j} \tag{20}$$

where high order terms such as $(V'_{i,j})^2$ have been neglected. Substituting Eq. (20) into Eq. (3), in addition to decomposing $U_{i-\frac{1}{2}}$ and $P_{i,j}$, one gets,

$$(U^* + U')_{i-\frac{1}{2},j} = \hat{U}_{i-\frac{1}{2},j} + \hat{d}_{i-\frac{1}{2}}\left[P_{i-1,j} - (P^* + P')_{i,j}\right] + \frac{(V_{i-1,j} + V^*_{i,j})^2}{4a^u_{1-\frac{1}{2}}r_{1-\frac{1}{2}}} + \frac{(V_{i-1,j} + V^*_{i,j})}{2a^u_{1-\frac{1}{2}}r_{1-\frac{1}{2}}}V'_{i,j} \tag{21}$$

Again for a given set of guessed or "starred" variables, Eq. (3) yields a residue related to this approximate value such that,

$$U^*_{i-\frac{1}{2},j} = \hat{U}_{i-\frac{1}{2},j} + \hat{d}_{i-\frac{1}{2}}\left[P_{i-1,j} - (P^* + P')_{i,j}\right] + \frac{(V_{i-1,j} + V^*_{i,j})^2}{4a^u_{i-\frac{1}{2}}r_{i-\frac{1}{2}}} - R_{i-\frac{1}{2},j} \tag{22}$$

Subtracting Eq. (22) from Eq. (21), Eq. (19) is similarly obtained.

Now, substituting Eqs. (15) into corresponding Eqs. (16), a system connecting the residuals and corrections can be written into matrix form as,

$$\begin{bmatrix} 1 & 0 & 0 & 0 & \hat{d}_{i-\frac{1}{2}} & -\hat{f}_{i-\frac{1}{2}} \\ 0 & 1 & 0 & 0 & -\hat{d}_{i+\frac{1}{2}} & -\hat{f}_{i+\frac{1}{2}} \\ 0 & 0 & 1 & 0 & \hat{d}_{j-\frac{1}{2}} & 0 \\ 0 & 0 & 0 & 1 & -\hat{d}_{j+\frac{1}{2}} & 0 \\ -F_{i+\frac{1}{2}} & F_{i-\frac{1}{2}} & -F_{j+\frac{1}{2}} & F_{j+\frac{1}{2}} & 0 & 0 \\ 0 & 0 & 0 & 0 & 0 & 1 \end{bmatrix} \begin{bmatrix} U'_{i-\frac{1}{2},j} \\ U'_{i+\frac{1}{2},j} \\ W'_{i,j-\frac{1}{2}} \\ W'_{i,j+\frac{1}{2}} \\ P'_{i,j} \\ V'_{i,j} \end{bmatrix} = \begin{bmatrix} R_{i-\frac{1}{2},j} \\ R_{i+\frac{1}{2},j} \\ R_{i,j-\frac{1}{2}} \\ R_{i,j+\frac{1}{2}} \\ R_{i,j} \\ R^{V}_{i,j} \end{bmatrix} \tag{23}$$

In Eq. (23) the influence of V on the cross-flow field is directly accounted for by the $\hat{f}$-terms in the U-equation. For the axial direction, the $\hat{f}$-terms are of null value. The reverse effect, or say the cross-flow influence on the tangential velocity field, is here not treated implicitly. This fact accounts for the "zeros" in the last row of the matrix in Eq. (23). The solution of system (23) is then easily obtained by first finding corrections for V, calculating then the pressure P and later the velocity components U and W.

Boundary conditions used were given velocity at the flow inlet and non-slip condition at chamber walls. For cells facing the outlet plane, overall mass-conservation balance in each computational cell was used to calculate the control-volume outgoing velocity. Initial null values were set for all velocities. Numerical implementation of boundary conditions was achieved, as usual, by maintaining the constant initial values at the boundaries, where applicable, or by updating them in each iterative sweep, as in the cases of outlet surfaces. Also, all computations below used a 18x36 grid equally distributed in the domain of calculation.

Results and Discussion

The algebraic equations for the three-dimensional velocity field were solved, in addition to the *fully-coupled* scheme here described, by performing outer iterations for the components V while keeping U, W and P from previous iteration. A *line-by-line* smoothing operator, fully described elsewhere (e.g. [4]), was used to relax V, being the cross-flow field (U,W) calculated by the locally-coupled method of [8]. This *segregated* solution was set in such a way that the same number of sweeps throughout the tangential and cross-flow fields was finally obtained. Since in the coupled scheme every sweep for U, W, and P also implies in smoothing out V errors, this procedure was found to be a reasonable way to fairly compare the two methods. Further, the same relaxation parameter α, defined by the expression $\phi = \phi^{old} + \alpha(\phi^{new} - \phi^{old})$ (α=0.45 for P,V and α=0.55 for U,W), was used in both schemes for the two inlet swirling strength investigated, namely $\omega^2 = 0.1$ and $\omega^2 = 1.$, where $\omega^2 = (V_{in}/W_{in})$ and V_{in} and W_{in} are the tangential and axial velocities at the inlet, respectively. For W_{in} and Reynolds number $Re=\rho W_{in}R/\mu$ the values 1 m/s and 10^3, respectively, where used.

Normalized residues for the tangential velocity field, R_V, and for the mass continuity equation, in its absolute (R_{ij}^{abs}) and relative form (R_{ij}^{rel}), can be defined as,

$$R_V = \left\{ \sum_{ij} \left(R_{i,j}^V\right)^2 \Big/ (N \cdot M) \right\}^{\frac{1}{2}} ; \; R_{ij}^{abs} = \left\{ \sum_{ij} \left(F_{out} - F_{in}\right)_{ij}^2 \Big/ (N \cdot M) \right\}^{\frac{1}{2}} ; \; R_{ij}^{rel} = \left\{ \sum_{ij} \left(\frac{F_{out} - F_{in}}{F_{out} + F_{in}} \right)_{ij}^2 \Big/ (N \cdot M) \right\}^{\frac{1}{2}} \quad (24)$$

where N and M are the number of cells in the r- and z-directions, respectively. Also, F_{out} and F_{in} are the cell outgoing and incoming mass fluxes, respectively.

Residue histories for the tangential velocity field are presented in FIG. 2*a*. *Implicit* treatment of the tangential- cross-flow coupling implies in a greater error reduction during the first few iterations, but subsequently a more or less equivalent rate of decrease has been obtained by the two methods. A primary consequence of that is a relatively longer computer time when the decoupled solution is used with the same convergency criterium applied to the V-equation. The effect of different swirling strengths is also shown in the figure. Difficulties in obtaining numerical solutions at a higher swirl are indicated by the reduction on the rate of decrease of R_V for iteration number greater than about 700 in FIG. 2*a*

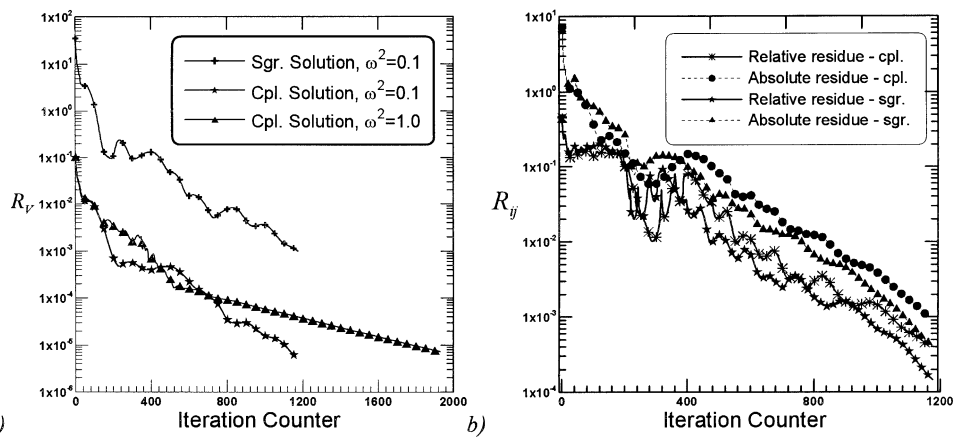

FIG. 2

Residue history: *a)* Tangential velocity equation, *b)* Mass residue for segregated and coupled methods.

Accompanying results for the mass residuals in both absolute and relative forms are presented in FIG. 2*b*. Both residuals for the *coupled* and *segregated* solutions present a consistent reduction throughout the iterations. Recalling now the results for R_V (FIG. 2*a*), the figures seem to indicate that the flow field can quickly adjust itself to changes in the tangential velocity profile, and that, in the segregated case, those changes are too slowly transferred to the tangential component V. The coupled solution, however, quickly transmits back to the V-equation changes in the cross-flow pattern, more realistic simulating the strong interaction among the variables involved.

Concluding Remarks

This paper detailed a fully-coupled technique for numerical prediction of confined swirling flows in a model combustor. An extension of the numerical method in [10] towards a fully implicit solution of the tangential and cross-flow equations was reported. Outline of the numerical method showed the necessary steps for setting up the residuals and the methodology used to calculate the corrections for all dependent variables. Comparison of segregated and fully- coupled treatments for the tangential velocity shows that the necessary computer effort is lower when the latter method was used. The approach herein is promising regarding numerical stability of the entire equation set since inherent coupling among the variables is handled implicitly. Further, it is also expected that more advanced multi-processor computer architectures can benefit from the point-wise error smoothing operator here proposed. Ultimately, distinct blocks of cells could be handled simultaneously by different processors, using each unit the methodology here described. Such solution methodology might contribute to reducing the overall computational time when numerically solving swirling flows.

Acknowledgements

The author is thankful to CNPq, Brazil, for their financial support during the course of this research.

References

1. S. Hogg, M.A. Leschiziner, *Int. J. Heat and Fluid Flow* **10**(1), 16 (1989).
2. S. Hogg, M.A. Leschiziner, *AIAA J.* **27**(1), 57 (1989).
3. M. Nikjook, H.C. Mongia, *Int. J. Heat and Fluid Flow* **12**(1), 12 (1991).
4. S.V. Patankar, *Numerical Heat Transfer and Fluid Flow*, Mc-Graw Hill:New York (1980).
5. S.V. Patankar, *Num. Heat Transf.* **4**, 409 (1981).
6. Patankar, S.V., Parabolic Systems, in W.J. Minkowycs, E.M. Sparrow, G.E. Scheider, and R.H. Pletcher (eds.), *Handbook of Numerical Heat Transfer*, chap. 2, Wiley, New York (1988).
7. M.J.S. de Lemos, Computation of Laminar Axi-Symmetric Recirculating Flows Using Primitive Variables and a Block-Implicit Scheme, *Proc. ENCIT90 - 3rd Braz. Therm. Sci. Meeting*, Itapema, SC, Brazil, vol. 1, pp. 375-380, December 10-12 (1990).
8. M.J.S. de Lemos, Simulation of Swirling Flow in A Model Combustor Using A Locally-Coupled Numerical Method, *Proc. of Winter Annual Meeting of the ASME*, Anaheim, CA, USA, vol. ASME-HTD-226, pp. 79-84, November 8-13 (1992).
9. S.P. Vanka, *J. Comp. Phys* **65,** 138 (1986).
10. S.P. Vanka, *Comp. Meth. App. Mech. Eng.* **55,** 321 (1986).
11. J.A. Rabi and M.J.S. de Lemos, *Applied Mathematics and Computation* **124**(2), 215 (2001).
12. M.J.S. de Lemos, *Numerical Heat Transfer - Part B* **37**(4), 489 (2000).

Received November 26, 2002